

Ammonia Synthesis From Water and Nitrogen Using Lanthanum-Doped Strontium Titanate/Gadolinium And Calcium Co-Doped Ceria Composite-Based Electrocatalyst

Ibrahim A. Amar^{1,*} 

¹ Department of Chemistry, Faculty of Science, Sebha University, Sebha/Libya

* Correspondence: ibr.amar@sebhau.edu.ly (I.A.A.);

Scopus Author ID 36968572200

Received: 31.08.2022; Accepted: 7.10.2022; Published: 16.11.2022

Abstract: Electrochemical synthesis of carbon-free ammonia from H₂O and N₂ is a promising technology for reducing global CO₂ emissions from the Haber-Bosch process (industrial ammonia production process). This study aims to explore the electrocatalyst activity of non-noble metal perovskite-based catalyst (La_{0.3}Sr_{0.7}TiO₃-Ce_{0.8}Gd_{0.18}Ca_{0.02}O_{2-δ}, LST-CGDC) for ammonia synthesis from wet nitrogen (3% H₂O). LST was prepared *via* a sol-gel process and characterized using X-ray diffraction (XRD). Ammonia was successfully synthesized in a double-chamber reactor, with a maximum ammonia formation rate of about 7×10^{-11} mol s⁻¹ cm⁻² and Faradaic efficiency of 0.2% at 400 °C and 1.4 V. The results demonstrated that direct ammonia synthesis from water and nitrogen is a promising green and sustainable ammonia synthesis technology.

Keywords: ammonia electrosynthesis; water; nitrogen; lanthanum-doped strontium titanate; redox stable perovskite oxide; carbon-free synthesis; composite cathodes

© 2022 by the authors. This article is an open-access article distributed under the terms and conditions of the Creative Commons Attribution (CC BY) license (<https://creativecommons.org/licenses/by/4.0/>).

1. Introduction

Ammonia (NH₃), after sulfuric acid (H₂SO₄), is ranked as the second most produced commodity, with about 160 million tons worldwide production [1,2]. Around (~ 88%) of the produced ammonia is used in the agricultural industry to make fertilizers to sustain global food production because of the world's population growth, which will result in more demand for ammonia. The rest is consumed to manufacture other commodities (e.g., synthetic fibers, explosives, pharmaceuticals, refrigerants, nitric acid, dyes, plastics, resins, and cleaning products) [1-5]. In addition, carbon-free ammonia is becoming more popular as an ideal energy carrier and hydrogen source (H₂ content 17.6% by weight) [6,7].

Currently, industrial ammonia production (> 70%) relies predominantly on the Haber-Bosch process (H-B), which was developed in the early 1900s [8,9]. In this process, ammonia is produced from its precursors (H₂ and N₂, 3:1) at high temperature (400-500 °C) and pressure (up to 300 bar) over an iron-based catalyst with a low conversion (10-15%) [6]. The required hydrogen for this energy-intensive process is produced through the steam reforming of fossil fuel feedstocks (coal or natural gas). This process is responsible for 1-2% world's energy consumption, ~ 1.5 greenhouse gas emissions, ~ 400 annual million tons of CO₂ emissions, and 2-5% of global natural gas consumption [3,8,10]. As the demand for ammonia grows, it is of great need to develop alternative approaches that consume less energy and are carbon-free

to produce green ammonia [11]. Besides, using green ammonia as clean fuel could reduce 50% of carbon emissions from shipping by 2050 [12].

The electrosynthesis of ammonia has the potential to overcome the main limitations of the Haber-Bosch process, including low ammonia conversion, high energy consumption, and severe environmental pollution [11,13-16]. Following the electrochemical synthesis of ammonia from its elements (H_2 and N_2) at atmospheric pressure by Marnellos and Stoukides in 1998 [13], many researchers have made significant efforts to synthesize ammonia electrochemically [17-20]. Despite its associated problems (i.e., production, storage, and transportation) [8,21,22], pure H_2 was used as an ammonia precursor in those studies. Hence, industrial and carbon-free societies paid more attention to using water as an alternative source of H_2 and renewable electricity (e.g., wind and solar) for the ammonia synthesis process (carbon-free ammonia synthesis) [3,23].

The electrosynthesis of ammonia from steam, hydrogen source, and nitrogen at atmospheric pressure was first reported by Skodra and Stoukides in 2009 [24]. In that study, ammonia was produced in an electrolytic cell based on Ru-MgO, a precious metal-based catalyst, and either proton (H^+) or oxygen-ion (O^{2-}) conducting electrolyte. Ammonia was synthesized successfully with a formation rate of about $3.75 \times 10^{-13} \text{ mol s}^{-1} \text{ cm}^{-2}$ at 650°C . This low ammonia formation rate was attributed to the low electronic conductivity of the Ru-MgO catalyst. The principle of ammonia synthesis from water and nitrogen in an electrolytic cell based on an oxygen-ion (O^{2-}) conducting electrolyte is represented in Figure 1.

In the electrochemical processes, material selection for designing an electrocatalyst (working electrode) is challenging [25]. In the literature, different electrocatalyst materials, including noble metals (Pt, Ag, and Ru), have been used for the electrochemical synthesis of ammonia directly from H_2O and N_2 [24,26,27], metal-organic-frame work (MOF) [28] spinels [29,30], perovskites [26,31,32] and perovskite-nitride composite [25]. However, selective nitrogen reduction reaction (NRR) electrocatalysts that support ammonia formation and suppress the strong competitive hydrogen evolution reaction (HER) remain elusive [33].

Perovskite-type oxides are of great interest owing to their properties such as good electrocatalytic activity, ease of synthesis, mixed electronic-ionic conductivities, low-cost compared to noble metals, flexibility, and excellent stability [18,25,34,35]. Among the perovskites, lanthanum doped strontium titanate ($\text{La}_x\text{Sr}_{1-x}\text{O}_3$, LST), Co and Fe-free and non-noble containing oxide, has attracted more attention due to its thermal stability, redox stability, chemical stability, sulfur resistance, carbon deposition resistance, mixed electronic and ionic conduction [36-41]. These properties make LST-based materials promising anodes for solid oxide fuel cells (SOFCs) [36,37,42] and direct carbon fuel cells (DCFCs) [43], and cathodes for solid oxide electrolysis cells (SOECs) [39-41] and solid-state ammonia synthesis (SSAS) [32,44]. In addition to their previous properties, it was also reported that LST-based cathodes exhibited good performance in a reducing gas-free atmosphere and without cathode pre-reduction during H_2O and CO_2 electrolysis [41]. This feature makes LST also a promising cathode for direct electrochemical synthesis of ammonia from H_2O and N_2 . In a previous study, precious metal-containing La-doped SrTiO_3 ($\text{La}_{0.3}\text{Sr}_{0.6}\text{Ti}_{0.6}\text{Ru}_{0.4}\text{O}_3$, LSTR) was employed as a cathode for ammonia synthesis from H_2O and N_2 in electrolytic cell based on proton-conducting (H^+) electrolyte [32].

In this study, a composite cathode $\text{La}_{0.3}\text{Sr}_{0.7}\text{TiO}_3\text{-Ce}_{0.8}\text{Gd}_{0.18}\text{Ca}_{0.02}\text{O}_{2-\delta}$ (LST-CGDC) was used as an electrocatalyst for direct ammonia synthesis from H_2O and N_2 in electrolytic cell based on oxygen-ion (O^{2-}) electrolyte (CGDC-(Li/Na/K) $_2\text{CO}_3$), with no cathode (LST-

CGDC) pre-reduction step. Besides, CGDC-ternary carbonate and $\text{Sr}_{0.5}\text{Sm}_{0.5}\text{CoO}_{3-\delta}$ (SSCo), respectively, were selected as an electrolyte and anode due to their high oxygen-ion conductivity [29] and oxygen evolution reaction (OER) activity [45].

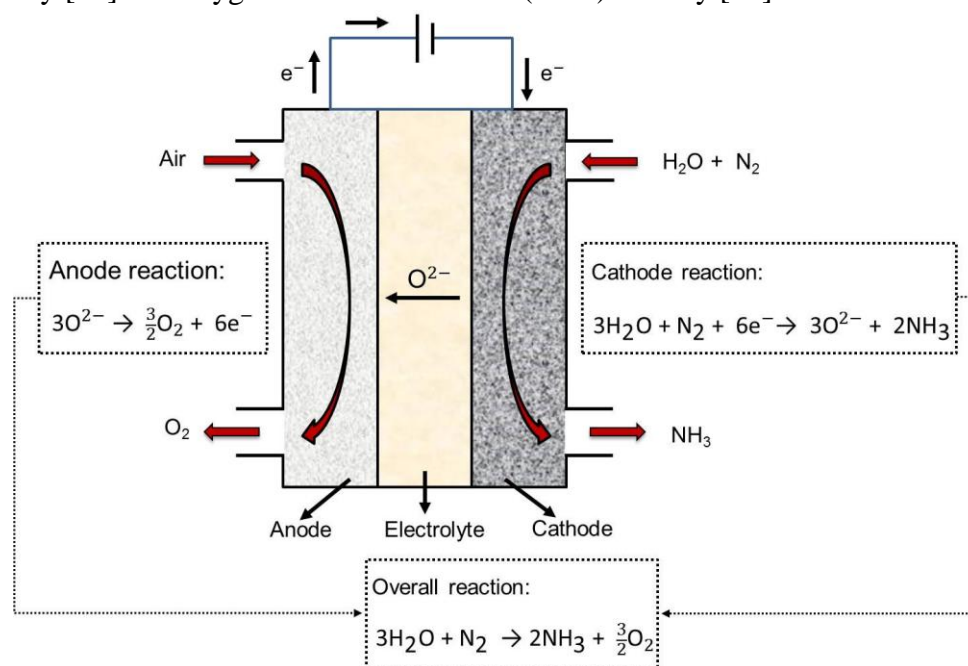


Figure 1. The principle of ammonia synthesis from water and nitrogen in a double-chamber reactor based on oxygen-ion (O^{2-}) conducting electrolyte

2. Materials and Methods

2.1. Chemicals.

Titanium (IV) isopropoxide ($\text{C}_{12}\text{H}_{28}\text{O}_4\text{Ti}$, 97+%), lanthanum oxide (La_2O_3 , 99%), gadolinium oxide (Gd_2O_3 , 99.9%), cerium nitride hexahydrate ($\text{Ce}(\text{NO}_3)_3 \cdot 6\text{H}_2\text{O}$, 99%), calcium nitrate tetrahydrate ($\text{Ca}(\text{NO}_3)_2 \cdot 4\text{H}_2\text{O}$, 99%), ethylenediaminetetraacetic acid, EDTA, ($\text{C}_{10}\text{H}_{18}\text{N}_2\text{O}_8$, 99%), strontium nitrate ($\text{Sr}(\text{NO}_3)_2$, 99%), lithium carbonate (Li_2CO_3 , 98%), potassium carbonate (K_2CO_3 , 99%), samarium oxide (Sm_2O_3 , 99.9%), and citric acid ($\text{C}_6\text{H}_8\text{O}_7$, 99%), were purchased from Alfa Aesar. Sodium carbonate (Na_2CO_3 , 99.5%) and cobalt nitrate hexahydrate ($\text{Co}(\text{NO}_3)_2 \cdot 6\text{H}_2\text{O}$, 98%) were purchased from Sigma Aldrich. Nitric acid (HNO_3 , 70%) and ammonia solution (NH_3 , 35%) were purchased from Fisher.

2.2. Materials synthesis.

This study synthesized the electrocatalyst ($\text{La}_{0.3}\text{Sr}_{0.7}\text{TiO}_3$, LST) *via* an EDTA-citric acid complexing sol-gel process, as described elsewhere [46]. In brief, the required amounts of $\text{C}_{12}\text{H}_{28}\text{O}_4\text{Ti}$, $\text{Sr}(\text{NO}_3)_2$, La_2O_3 (HNO_3 solution was used to convert it to nitrate form), and $\text{Sr}(\text{NO}_3)_2$ were dissolved in deionized water. The complexing agents (citric acid and EDTA) were then added in a 1.5:1:1 molar ratio (citric acid:EDTA:total metal ions). The ammonia solution was then added to the mixture until the pH reached 6, after which it was evaporated on a hot plate under stirring to induce gelation. The formed gel was dried further before being calcined in air at 900 °C for 2 hours to produce LST powder. Ca and Gd co-doped ceria ($\text{Ce}_{0.8}\text{Gd}_{0.18}\text{Ca}_{0.02}\text{O}_{2-\delta}$, CGDC) and $\text{Sm}_{0.5}\text{Sr}_{0.5}\text{CoO}_{3-\delta}$ (SSCo) powders were also synthesized *via* the above mentioned sol-gel process [29]. Solid-state reaction (SSR) was used to prepare the composite electrolyte (CGDC/ $(\text{Li}/\text{Na}/\text{K})_2\text{CO}_3$ 70:30 wt%), as described elsewhere [29].

2.3. Materials characterization.

The phase purity of the prepared materials was examined using a Panalytical X'Pert Pro diffractometer with CuK α radiation ($\lambda=1.5405 \text{ \AA}$), at 40 kV and 40 mA and in the 2θ range between 5-100°. The lattice parameters ($a = b = c$) and crystallite size (D) were estimated using the following equations [47];

$$a = d_{hkl} \sqrt{h^2 + k^2 + l^2} \quad (1)$$

$$D = \frac{0.9\lambda}{(\beta \cos\theta)} \quad (2)$$

where, d is the spacing between crystal planes, hkl are the Miller indices, λ is the X-ray wavelength θ is Bragg's diffraction angle, and β is the full width at half maximum (FWHM).

2.4. Fabrication of the single-cell.

In this study, the electrolytic cell (single-cell) used for ammonia synthesis was fabricated as described elsewhere [29]. In this cell (SSCo-CGDC|CGDC-carbonate|LST-CGDC), the anode, electrolyte, and cathode were composed of SSSCo-CGDC (70:30 wt%), CGDC-carbonate (70:30 wt%) and LST-CGDC (70:30 wt%), respectively. In addition, starch (15 wt%) was added to both electrodes as a pore former. The single-cell components (anode, electrolyte, and cathode) were pressed into a 19 mm pellet at 121 MPa before being sintered in air at 700 °C for 2 h. The geometric surface area of the cathode was 0.785 cm². A silver paste was used to make the electrodes' current collectors (in a grid pattern), and Ag wires were attached to both electrodes to serve as output terminals.

2.5. Ammonia synthesis.

This study synthesized ammonia using a self-designed double-chamber reactor, as described elsewhere [29]. In brief, the cathode chamber was fed wet N₂ (3% H₂O), while the anode chamber was exposed to air. A potentiostat/galvanostat (Solartron 1287A) was used for the ammonia synthesis experiments to apply a constant voltage across the electrolytic cell for 30 minutes. The ammonia produced at the cathode chamber was absorbed using 20 mL of HCl solution (0.1 mol L⁻¹). The NH₄⁺ concentration was estimated using an ion-selective electrode (ISE, Orion Star A214). The following equations were used to calculate the ammonia formation rate and the Faradaic efficiency [18,48];

$$r_{\text{NH}_3} = \frac{c_{\text{NH}_4^+} \times V}{M_{\text{NH}_4^+} \times t \times A} \quad (3)$$

$$\text{Faradaic efficiency (\%)} = \frac{3F \times r_{\text{NH}_3}}{I} \times 100 \quad (4)$$

where r_{NH_3} is the rate of ammonia formation (mol s⁻¹ cm⁻²), $M_{\text{NH}_4^+}$ is the molar mass of NH₄⁺ (18 g mol⁻¹), V is the volume of HCl solution (20 mL), t (s) is ammonia collection time, $c_{\text{NH}_4^+}$ is NH₄⁺ ion concentration (g mL⁻¹), A is the cathode geometric surface area (0.785 cm²), F is the Faradaic constant, and I is the generated current density (mA cm⁻²).

3. Results and Discussion

3.1. Characterization.

The XRD pattern of La-doped SrTiO₃ (La_{0.3}Sr_{0.7}TiO₃, LST) after calcinating its dried gel precursor in the air at 900 °C for 2 h is shown in Figure 2b. As can be seen, a single phase of LST was obtained, and all the diffraction peaks are indexed well to the standard SrTiO₃ (Figure 2a) with a cubic perovskite structure (JCPDS No. 35-0734) [49]. The lattice constant ($a = b = c$) of LST, estimated from the most intense peak (110), was found to be 3.8953 Å. This value is similar to those reported by others for La-doped SrTiO₃ (3.8876-3.9075 Å) [39,40,50]. The crystallite size (D) of LST was approximately 23.31 nm.

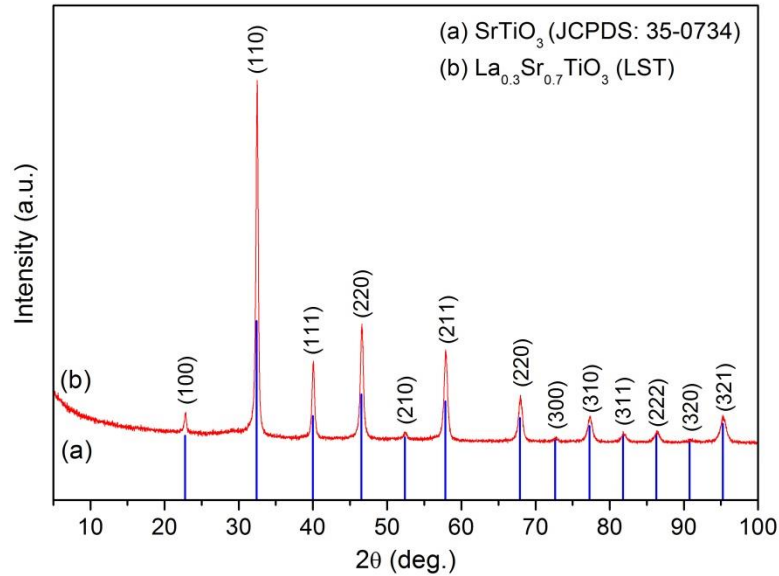


Figure 2. XRD pattern: (a) La_{0.3}Sr_{0.7}TiO₃ (LST) after firing its dried gel in the air at 900 °C for 2 h; (b) SrTiO₃ standard.

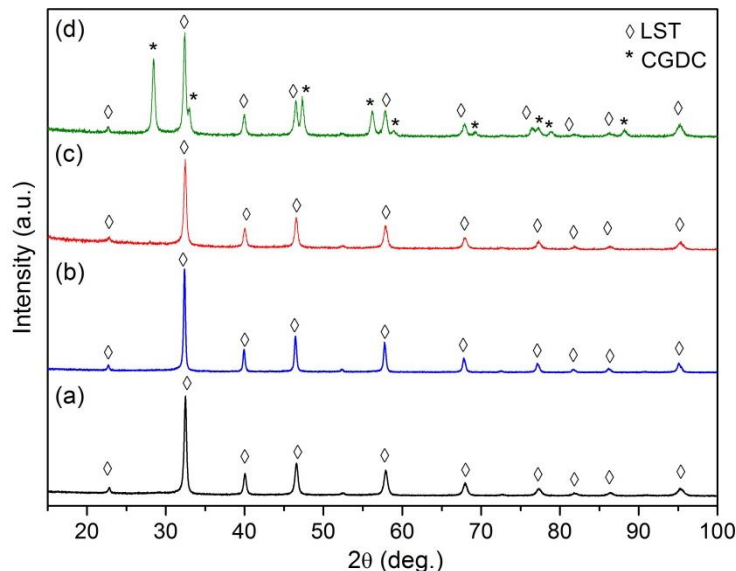


Figure 3. XRD pattern: (a) La_{0.3}Sr_{0.7}TiO₃ (LST); (b) LST after heat treatment in 5% H₂-Ar at 1200 °C for 5 h.; (c) LST after heat treatment in N₂ at 500 °C; (d) LST-CGDC composite fired in the air at 700 °C for 30 min.

Figures 3a-d show the XRD patterns of LST, LST fired in 5% H₂-Ar (reducing atmosphere) at 1200 °C for 5 h, LST fired in N₂ at 500 °C and LST-CGDC composite fired in the air at 700 °C, respectively. As shown, the LST sample retained its perovskite structure, and no phase change was observed after being heated at 1200 °C for 5 h in 5% H₂-Ar (Figure 3b)

and N₂ at 500 °C (Figure 3c). Furthermore, the lattice constant ($a = b = c$) of the LST sample that was heated in 5% H₂-Ar (3.9082 Å) and N₂ (3.8983 Å) was similar to that of the as-synthesized LST sample (3.8953 Å), indicating its stability in both atmospheres. For the composite cathode (LST-CGDC), its XRD pattern exhibits only the peaks belonging (no additional peaks observed) to the LST and CGDC after firing the composite cathode at the single-cell sintering temperature (700 °C) in the air for 30 min, as shown in Figure 3d. This indicates that the composite cathode's components are chemically compatible at this temperature (700 °C).

3.2. Ammonia synthesis.

3.2.1. Ammonia synthesis at different temperatures.

Figure 4 displays the generated current density under the employed ammonia synthesis conditions (various operating temperatures ranging from 375 to 450 °C and a constant applied voltage of 1.4 V for 30 min). As shown from the figure, apart from the drop in generated current density at the initial stage (~ 2 min), almost a constant current density was observed at all operating temperatures, indicating short-term performance stability of the electrolytic cell under these conditions for ammonia synthesis. This observed initial drop in the generated current density is due to the blocking effect of charged ions that accumulated at the interfacial region between the electrodes and electrolyte, as reported by others [28,51]. In this case, the transferred oxygen-ions (O²⁻) across the electrolyte may partially be blocked by the positively charged ions (e.g., Li⁺, Na⁺, K⁺) that accumulated the electrolyte/cathode interface, which in turn results in current density decline [52]. Furthermore, by raising the electrolytic cell operating temperature from 375 to 450 °C, a significant increase in generated current density was attained, reaching the highest value of about 23.36 mA cm⁻² at 450 °C, as shown in Figure 4. This increase in the generated current density with a cell operating temperature increase is due to the enhancement of the ionic conductivity of the composite electrolyte [29].

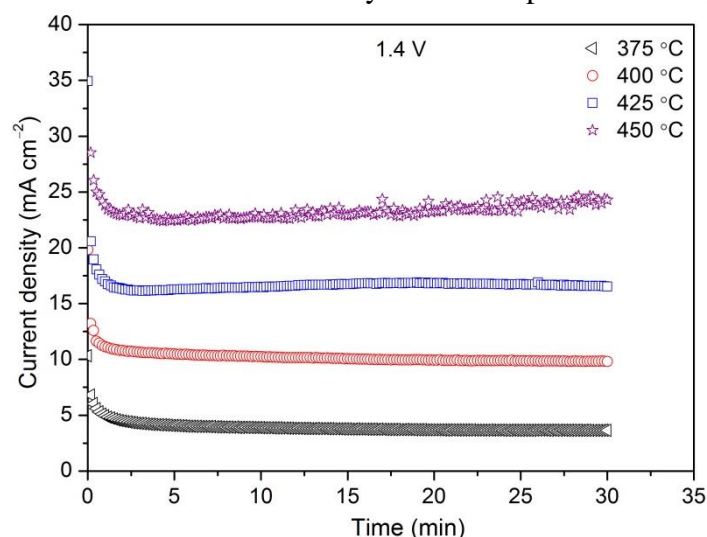


Figure 4. Generated current density-time curve during the synthesis of ammonia from water and nitrogen at various operating temperatures and applied voltage of 1.4 V.

Figure 5 shows the effect of the rate of ammonia formation and its corresponding Faradaic efficiency on the cell operating temperature (375-450 °C) when a constant voltage of about 1.4 was applied across the electrolytic cell for 30 min. As shown, a significant increase in the ammonia formation and its corresponding Faradaic efficiency was observed with

increasing the cell operating temperature from 375 to 400 °C. However, a further increase in cell operating temperature (> 400 °C) resulted in a significant decline in the ammonia formation rate and the Faradaic efficiency. This decrease in ammonia formation is due to increased ammonia decomposition at high operating temperatures [26]. In this study, 400 °C seems to be the optimum cell operating temperature at which the highest ammonia production rate of about $7 \times 10^{-11} \text{ mol s}^{-1} \text{ cm}^{-2}$ with Faradaic efficiency of approximately 0.2% was attained. This ammonia formation rate is higher than that reported for precious metal-containing perovskite oxide, $\text{La}_{0.3}\text{Sr}_{0.6}\text{Ti}_{0.6}\text{Ru}_{0.4}\text{O}_3$, ($3.8 \times 10^{-12} \text{ mol s}^{-1} \text{ cm}^{-2}$ at 500 °C) [32].

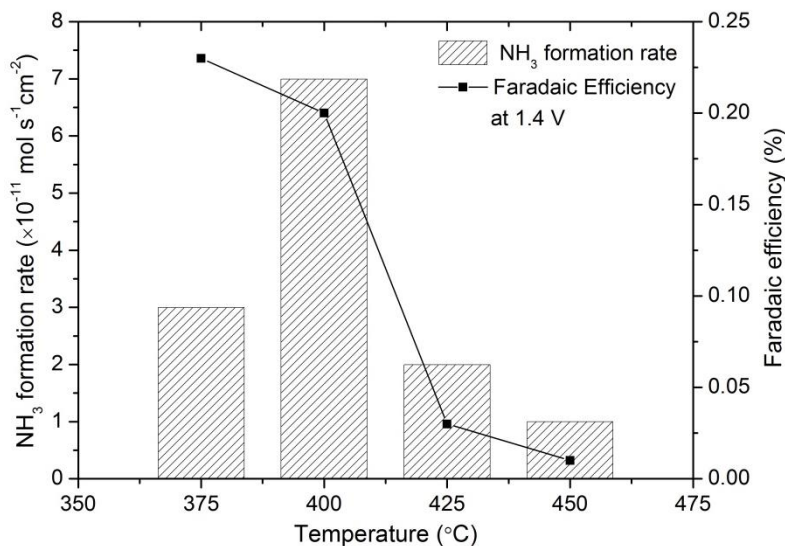


Figure 5. The effect of cell operating temperature on ammonia formation rate.

3.2.2. Ammonia synthesis at different applied voltages

Figure 6 shows the reported generated current density during the electrosynthesis of ammonia under various applied voltages ranging from 1.2 to 1.8 V and a fixed cell operating temperature of 400 °C for 30 min.

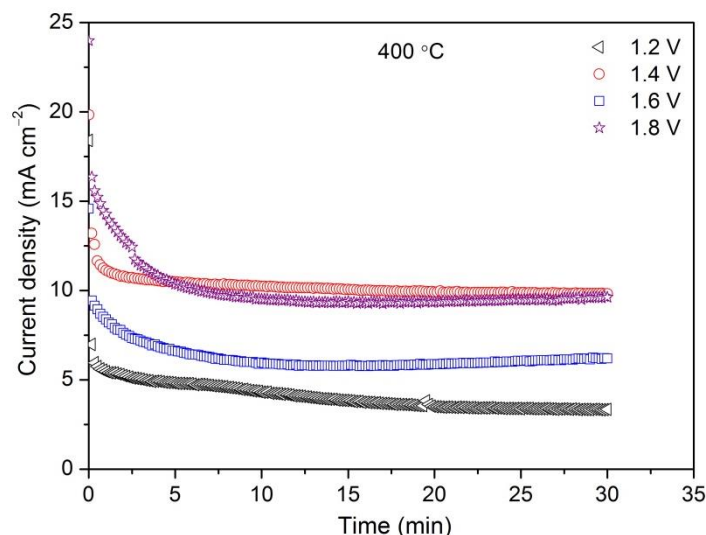


Figure 6. Generated current density-time curve during the synthesis of ammonia from water and nitrogen at various applied voltages and 400 °C.

As can be seen, the generated current density increased significantly from 3.68 to 10.12 mA cm⁻² when the electrolytic cell was operated at 1.2 and 1.4 V, respectively. However, at high applied voltages (> 1.4 V), there was a decline in the generated current density, reaching

a low value of about 6.03 mA cm^{-2} at 1.6 V. This observed decrease in the generated current density is due to the ion-blocking effect as mentioned previously [28,51,52]. Although the decrease in the generated current densities was observed at high applied voltages (1.6 and 1.8 V), the electrolytic cell exhibited almost stable performance at all applied voltages (1.2-1.8 V), indicating its short-term performance stability.

Figure 7 shows the effect of the applied voltages (1.2-1.8 V) on the ammonia production rate and its corresponding Faradaic efficiency at fixed cell operating temperature ($400 \text{ }^\circ\text{C}$). It was observed that the rate of ammonia formation increased significantly with increasing the applied voltages, reaching a maximum value ($7 \times 10^{-11} \text{ mol s}^{-1} \text{ cm}^{-2}$) at an applied voltage of 1.4 V. However, a further increase in the applied voltage from 1.6 to 1.8 V resulted in a significant decrease in the ammonia formation rate to almost a constant value ($\sim 1 \times 10^{-11} \text{ mol s}^{-1} \text{ cm}^{-2}$). This decrease in the rate of ammonia formation could be attributed to the observed decrease in the generated current density, as mentioned above [53]. Besides, at all applied voltages, very low corresponding Faradaic efficiency was attained ($< 1\%$), which implies that most of the supplied energy was consumed in the competing hydrogen evolution reaction (HER), as observed by others [18,54].

Table 1 compares the rate of ammonia production from water (H_2O) and nitrogen (N_2) using various electrocatalysts to that observed by the prepared composite cathode (LST-CGDC). As shown in the table, the proposed electrocatalyst has a higher ammonia formation rate than noble metal-based catalysts (Ru, Ag, and Pt) [24,26] or $\text{La}_{0.3}\text{Sr}_{0.6}\text{Ti}_{0.6}\text{Ru}_{0.4}\text{O}_3$ (noble metal-containing perovskite oxide) [32] and comparable to that observed using spinel based oxides [29,30]. Besides, it can also be seen from the table that the ammonia formation rate obtained using LST-CGDC was lower than the reported for the noble metal-free-perovskite oxides ($\text{La}_{0.75}\text{Sr}_{0.25}\text{Cr}_{0.5}\text{Fe}_{0.5}\text{O}_{3-\delta}$ and $\text{La}_{0.8}\text{Cs}_{0.2}\text{Fe}_{0.8}\text{Ni}_{0.2}\text{O}_{3-\delta}$) [55,56] and metal-organic-framework (MOF)-based catalysts [28]. In general, the listed electrocatalyst exhibited low Faradaic efficiencies ($< 4\%$), indicating that the competing hydrogen evolution reaction (HER) is the dominating process. Thus, finding an efficient electrocatalyst that supports ammonia production and suppresses HER is of crucial importance. Furthermore, despite their low Faradaic efficiency, precious metal-free perovskite oxides are more affordable than noble metal-based electrocatalysts.

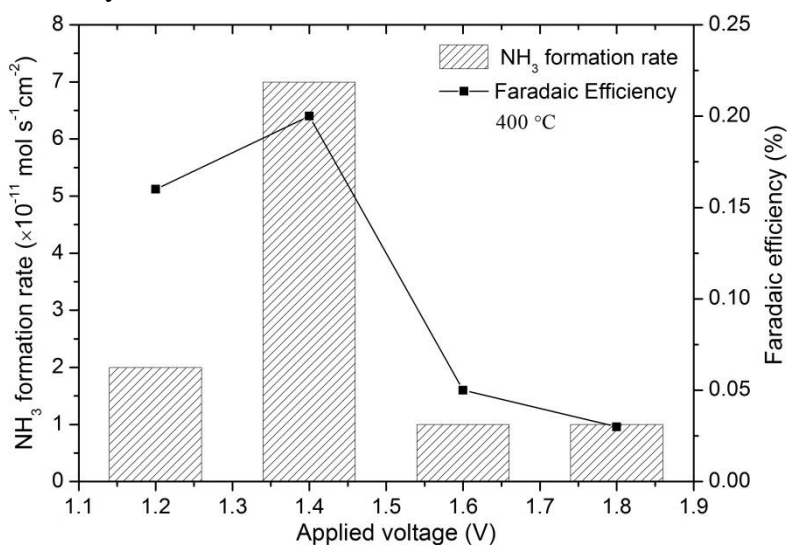


Figure 7. The effect of the applied voltage on ammonia formation rate.

Table 1. This is a table. Tables should be placed in the main text near the first time they are cited.

Electrocatalyst	Applied voltage (V)	T (°C)	r_{NH_3} (mol s ⁻¹ cm ⁻²)	Faradaic Efficiency (%)	Ref
Ru-based catalyst	2	650	3.75×10^{-13}	-	[24]
Pt	0.8	550	$< 1 \times 10^{-12}$	-	[26]
La _{0.3} Sr _{0.6} Ti _{0.6} Ru _{0.4} O ₃	- 0.1	500	3.8×10^{-12}	-	[32]
Ag	0.8	550	4.9×10^{-11}	0.46	[26]
CoFe _{1.9} Mo _{0.1} O ₄ -Ce _{0.8} Gd _{0.18} Ca _{0.02} O _{2-δ}	1.4	400	6×10^{-11}	0.11	[30]
CoFe ₂ O ₄ -Ce _{0.8} Gd _{0.18} Ca _{0.02} O _{2-δ}	1.6	400	6.5×10^{-11}	0.17	[29]
La _{0.3} Sr _{0.7} TiO ₃ -Ce _{0.8} Gd _{0.18} Ca _{0.02} O _{2-δ} (LST-CGDC)	1.4	400	7×10^{-11}	0.2	This study
La _{0.6} Sr _{0.4} Co _{0.2} Fe _{0.8} O _{3-δ}	0.8	550	8.5×10^{-11}	0.33	[26]
LaFeO ₃	2	80	1.26×10^{-10}	0.32	[56]
Pt/C-loaded carbon paper	1.2	220	2×10^{-10}	2.1	[27]
La _{0.75} Sr _{0.25} Cr _{0.5} Mn _{0.5} O _{3-δ} -Ce _{0.8} Gd _{0.18} Ca _{0.02} O _{2-δ}	1.4	400	2×10^{-10}	0.52	[31]
La _{0.8} Cs _{0.2} Fe _{0.8} Ni _{0.2} O _{3-δ}	2.4	80	3.52×10^{-10}	0.16	[56]
La _{0.75} Sr _{0.25} Cr _{0.5} Fe _{0.5} O _{3-δ} -Ce _{0.8} Gd _{0.18} Ca _{0.02} O _{2-δ}	1.4	375	4×10^{-10}	3.87	[55]
Metal-organic-framework, MOF(Fe)	1.2	90	2.12×10^{-9}	1.43	[28]

4. Conclusions

In summary, the activity of a composite cathode based on a non-noble metal, Co and Fe-free perovskite oxide (La_{0.3}Sr_{0.7}TiO₃-Ce_{0.8}Gd_{0.18}Ca_{0.02}O_{2-δ}, LST-CGDC) for ammonia synthesis electrochemically from H₂O and N₂ was successfully explored. The X-ray diffraction (XRD) was used to characterize La_{0.3}Sr_{0.7}TiO₃ (LST), which was synthesized *via* a sol-gel method. The XRD results revealed that after 2 h of calcination at 900 °C, a single-phase perovskite oxide (LST) with an average crystallite size of 23.31 nm was obtained. The XRD results also showed that the LST was stable in the reducing atmosphere (5% H₂-Ar). The results showed that ammonia could be successfully synthesized under atmospheric pressure from wet N₂ (3% H₂O) using LST-CGDC composite as an electrocatalyst. Furthermore, the maximum ammonia formation rate (7×10^{-11} mol s⁻¹ cm⁻²) and Faradaic efficiency (0.2%) were attained at a cell operating temperature of 400 °C and an applied voltage of 1.4 V. Despite the low Faradaic efficiency and ammonia formation rate; the findings showed that the prepared non-noble electrocatalyst (LST) is a promising material for carbon-free ammonia synthesis.

Funding

This research received no external funding.

Acknowledgments

The author would like to express his gratitude to Professor Shanwen Tao of the University of Warwick in Coventry, UK, for providing the necessary equipment for ammonia synthesis. The author would also like to express his gratitude to Dr. Rong Lan from Coventry University, Coventry, UK, for her assistance and encouragement. The authors would also like to thank the Department of Pure and Applied Chemistry at Strathclyde University in Glasgow, UK, for the XRD analysis.

Conflicts of Interest

The author declares no conflict of interest.

References

1. Survey, U.G. Mineral Commodity Summaries 2020: U.S. Geological Survey. **2020**, *200*, <https://doi.org/10.3133/mcs2020>.
2. Ghavam, S.; Vahdati, M.; Wilson, I.; Styring, P. Sustainable ammonia production processes. *Frontiers in Energy Research* **2021**, *34*, <https://doi.org/10.3389/fenrg.2021.580808>.
3. Zhang, T.; Zhou, R.; Zhang, S.; Zhou, R.; Ding, J.; Li, F.; Hong, J.; Dou, L.; Shao, T.; Murphy, A.B.; et al. Sustainable Ammonia Synthesis from Nitrogen and Water by One-Step Plasma Catalysis. *Energy & Environmental Materials* **2022**, <https://doi.org/10.1002/eem2.12344>.
4. Liu, H.; Guijarro, N.; Luo, J. The pitfalls in electrocatalytic nitrogen reduction for ammonia synthesis. *Journal of Energy Chemistry* **2021**, *61*, 149-154, <https://doi.org/10.1016/j.jechem.2021.01.039>.
5. Shen, H.; Choi, C.; Masa, J.; Li, X.; Qiu, J.; Jung, Y.; Sun, Z. Electrochemical ammonia synthesis: Mechanistic understanding and catalyst design. *Chem* **2021**, *7*, 1708-1754, <https://doi.org/10.1016/j.chempr.2021.01.009>.
6. Yüzbaşıoğlu, A.E.; Avşar, C.; Gezerman, A.O. The current situation in the use of ammonia as a sustainable energy source and its industrial potential. *Current Research in Green and Sustainable Chemistry* **2022**, *5*, 100307, <https://doi.org/10.1016/j.crgsc.2022.100307>.
7. Wang, B.; Li, T.; Gong, F.; Othman, M.H.D.; Xiao, R. Ammonia as a green energy carrier: Electrochemical synthesis and direct ammonia fuel cell - a comprehensive review. *Fuel Processing Technology* **2022**, *235*, 107380, <https://doi.org/10.1016/j.fuproc.2022.107380>.
8. Kurien, C.; Mittal, M. Review on the production and utilization of green ammonia as an alternate fuel in dual-fuel compression ignition engines. *Energy Conversion and Management* **2022**, *251*, 114990, <https://doi.org/10.1016/j.enconman.2021.114990>.
9. Liu, H. *Ammonia synthesis catalysts: innovation and practice*; World Scientific: 2013.
10. Yang, B.; Ding, W.; Zhang, H.; Zhang, S. Recent progress in electrochemical synthesis of ammonia from nitrogen: strategies to improve the catalytic activity and selectivity. *Energy & Environmental Science* **2021**, *14*, 672-687, <https://doi.org/10.1039/d0ee02263b>.
11. Lee, C.; Yan, Q. Electrochemical reduction of nitrogen to ammonia: Progress, challenges and future outlook. *Current Opinion in Electrochemistry* **2021**, *29*, 100808, <https://doi.org/10.1016/j.coelec.2021.100808>.
12. Smart, K. Review of Recent Progress in Green Ammonia Synthesis. *Johnson Matthey Technology Review* **2022**, *66*, 230-244, <https://doi.org/10.1595/205651322X16334238659301>.
13. Marnellos, G.; Stoukides, M. Ammonia synthesis at atmospheric pressure. *Science* **1998**, *282*, 98-100, <https://doi.org/10.1126/science.282.5386.98>.
14. Amar, I.A.; Lan, R.; Petit, C.T.G.; Tao, S. Solid-state electrochemical synthesis of ammonia: a review. *Journal of Solid State Electrochemistry* **2011**, *15*, 1845-1860, <https://doi.org/10.1007/s10008-011-1376-x>.
15. Garagounis, I.; Vourros, A.; Stoukides, D.; Dasopoulos, D.; Stoukides, M. Electrochemical Synthesis of Ammonia: Recent Efforts and Future Outlook. *Membranes* **2019**, *9*, <https://doi.org/10.3390/membranes9090112>.
16. Garagounis, I.; Kyriakou, V.; Skodra, A.; Vasileiou, E.; Stoukides, M. Electrochemical synthesis of ammonia in solid electrolyte cells. *Frontiers in Energy Research* **2014**, *2*, 1, <https://doi.org/10.3389/fenrg.2014.00001>.
17. Amar, I.A.; Petit, C.T.G.; Zhang, L.; Lan, R.; Skabara, P.J.; Tao, S. Electrochemical synthesis of ammonia based on doped-ceria-carbonate composite electrolyte and perovskite cathode. *Solid State Ionics* **2011**, *201*, 94-100, <https://doi.org/10.1016/j.ssi.2011.08.003>.
18. Kim, H.; Chung, Y.S.; Kim, T.; Yoon, H.; Sung, J.G.; Jung, H.K.; Kim, W.B.; Sammes, L.B.; Chung, J.S. Ru-doped barium strontium titanates of the cathode for the electrochemical synthesis of ammonia. *Solid State Ionics* **2019**, *339*, 115010, <https://doi.org/10.1016/j.ssi.2019.115010>.
19. Lei, Z.; Jing, J.; Pang, J.; Hu, R.; Shi, X.; Yang, Z.; Peng, S. Highly conductive proton-conducting electrolyte with a low sintering temperature for electrochemical ammonia synthesis. *International Journal of Hydrogen Energy* **2020**, *45*, 8041-8051, <https://doi.org/10.1016/j.ijhydene.2020.01.039>.
20. Klinsrisuk, S.; Irvine, J.T.S. Electrocatalytic ammonia synthesis via a proton conducting oxide cell with BaCe_{0.5}Zr_{0.3}Y_{0.16}Zn_{0.04}O_{3-δ} electrolyte membrane. *Catalysis Today* **2017**, *286*, 41-50, <https://doi.org/10.1016/j.cattod.2016.06.051>.
21. Dutta, S. A review on production, storage of hydrogen and its utilization as an energy resource. *Journal of Industrial and Engineering Chemistry* **2014**, *20*, 1148-1156, <https://doi.org/10.1016/j.jiec.2013.07.037>.
22. Jeerh, G.; Zhang, M.; Tao, S. Recent progress in ammonia fuel cells and their potential applications. *Journal of Materials Chemistry A* **2021**, *9*, 727-752, <https://doi.org/10.1039/d0ta08810b>.
23. Smith, C.; Hill, A.K.; Torrente-Murciano, L. Current and future role of Haber-Bosch ammonia in a carbon-free energy landscape. *Energy & Environmental Science* **2020**, *13*, 331-344, <https://doi.org/10.1039/c9ee02873k>.
24. Skodra, A.; Stoukides, M. Electrocatalytic synthesis of ammonia from steam and nitrogen at atmospheric pressure. *Solid State Ionics* **2009**, *180*, 1332-1336, <https://doi.org/10.1016/j.ssi.2009.08.001>.

25. Gunduz, S.; Deka, D.J.; Ferree, M.; Kim, J.; Millet, J.-M.M.; Co, A.C.; Ozkan, U.S. Composite Cathodes with Oxide and Nitride Phases for High-Temperature Electrocatalytic Ammonia Production from Nitrogen and Water. *ECS Advances* **2022**, *1*, 014501, <https://doi.org/10.1149/2754-2734/ac6618>.
26. Yun, D.S.; Joo, J.H.; Yu, J.H.; Yoon, H.C.; Kim, J.N.; Yoo, C.Y. Electrochemical ammonia synthesis from steam and nitrogen using proton conducting yttrium doped barium zirconate electrolyte with silver, platinum, and lanthanum strontium cobalt ferrite electrocatalyst. *Journal of Power Sources* **2015**, *284*, 245-251, <https://doi.org/10.1016/j.jpowsour.2015.03.002>.
27. Qing, G.; Kikuchi, R.; Kishira, S.; Takagaki, A.; Sugawara, T.; Oyama, S.T. Ammonia synthesis by N₂ and steam electrolysis in solid-state cells at 220 °C and atmospheric pressure. *Journal of the Electrochemical Society* **2016**, *163*, E282-E287, <https://doi.org/10.1149/2.0161610jes>.
28. Zhao, X.; Yin, F.; Liu, N.; Li, G.; Fan, T.; Chen, B. Highly efficient metal–organic-framework catalysts for electrochemical synthesis of ammonia from N₂ (air) and water at low temperature and ambient pressure. *Journal of Materials Science* **2017**, *52*, 10175-10185, <https://doi.org/10.1007/s10853-017-1176-5>.
29. Amar, I.A.; Petit, C.T.G.; Mann, G.; Lan, R.; Skabara, P.J.; Tao, S.W. Electrochemical synthesis of ammonia from N₂ and H₂O based on (Li,Na,K)₂CO₃-Ce_{0.8}Gd_{0.18}Ca_{0.02}O_{2-δ} composite electrolyte and CoFe₂O₄ cathode. *International Journal of Hydrogen Energy* **2014**, *39*, 4322-4330, <http://dx.doi.org/10.1016/j.ijhydene.2013.12.177>.
30. Amar, I.A.; Ahwidi, M.M. Electrocatalytic activity of CoFe_{1.9}Mo_{0.1}O₄-Ce_{0.8}Gd_{0.18}Ca_{0.02}O_{2-δ} composite cathode for ammonia synthesis from water and nitrogen. *World Journal of Engineering* **2021**, *18*, 490-496, <https://doi.org/10.1108/wje-07-2020-0270>.
31. Amar, I.A.; Ahwidi, M.M. Electrocatalytic Activity of Lanthanum Chromite-Based Composite Cathode for Ammonia Synthesis from Water and Nitrogen. *Advanced Materials Research* **2021**, *1160*, 65-74, <https://doi.org/10.4028/www.scientific.net/AMR.1160.65>.
32. Kosaka, F.; Noda, N.; Nakamura, T.; Otomo, J. In situ formation of Ru nanoparticles on La_{1-x}Sr_xTiO₃-based mixed conducting electrodes and their application in electrochemical synthesis of ammonia using a proton-conducting solid electrolyte. *Journal of Materials Science* **2017**, *52*, 2825-2835, <https://doi.org/10.1007/s10853-016-0573-5>.
33. Hao, Y.-C.; Guo, Y.; Chen, L.-W.; Shu, M.; Wang, X.-Y.; Bu, T.-A.; Gao, W.-Y.; Zhang, N.; Su, X.; Feng, X.; et al. Promoting nitrogen electroreduction to ammonia with bismuth nanocrystals and potassium cations in water. *Nature Catalysis* **2019**, *2*, 448-456, <https://doi.org/10.1038/s41929-019-0241-7>.
34. Zhang, M.; Jeerh, G.; Zou, P.; Lan, R.; Wang, M.; Wang, H.; Tao, S. Recent development of perovskite oxide-based electrocatalysts and their applications in low to intermediate temperature electrochemical devices. *Materials Today* **2021**, *49*, 351-377, <https://doi.org/10.1016/j.mattod.2021.05.004>.
35. Pecchi, G.; Jiliberto, M.; Delgado, E.; Cadús, L.; Fierro, J. Effect of B-site cation on the catalytic activity of La_{1-x}CaxBO₃ (B= Fe, Ni) perovskite-type oxides for toluene combustion. *Journal of Chemical Technology & Biotechnology* **2011**, *86*, 1067-1073, <https://doi.org/10.1002/jctb.2611>.
36. Li, X.; Zhao, H.; Zhou, X.; Xu, N.; Xie, Z.; Chen, N. Electrical conductivity and structural stability of La-doped SrTiO₃ with A-site deficiency as anode materials for solid oxide fuel cells. *International Journal of Hydrogen Energy* **2010**, *35*, 7913-7918, <https://doi.org/10.1016/j.ijhydene.2010.05.043>.
37. Presto, S.; Barbucci, A.; Carpanese, M.P.; Han, F.; Costa, R.; Viviani, M. Application of La-doped SrTiO₃ in advanced metal-supported solid oxide fuel cells. *Crystals* **2018**, *8*, 134, <https://doi.org/10.3390/cryst8030134>.
38. Liang, C.; Yang, C.; Wang, J.; Lin, P.; Li, X.; Wu, X.; Yuan, J. Sintering process and effects on LST and LST-GDC particles simulated by molecular dynamics modeling method. *Energies* **2020**, *13*, 4128, <https://doi.org/10.3390/en13164128>.
39. Gan, Y.; Qin, Q.; Chen, S.; Wang, Y.; Dong, D.; Xie, K.; Wu, Y. Composite cathode La_{0.4}Sr_{0.4}TiO_{3-δ}-Ce_{0.8}Sm_{0.2}O_{2-δ} impregnated with Ni for high-temperature steam electrolysis. *Journal of Power Sources* **2014**, *245*, 245-255, <https://doi.org/10.1016/j.jpowsour.2013.06.107>.
40. Tsekouras, G.; Irvine, J.T. The role of defect chemistry in strontium titanates utilised for high temperature steam electrolysis. *Journal of Materials Chemistry* **2011**, *21*, 9367-9376, <https://doi.org/10.1039/C1JM11313E>.
41. Li, S.; Li, Y.; Gan, Y.; Xie, K.; Meng, G. Electrolysis of H₂O and CO₂ in an oxygen-ion conducting solid oxide electrolyzer with a La_{0.2}Sr_{0.8}TiO_{3+δ} composite cathode. *Journal of Power Sources* **2012**, *218*, 244-249, <https://doi.org/10.1016/j.jpowsour.2012.06.046>.
42. Singh, S.; Pandey, R.; Verma, O.N.; Singh, P. Development of La and Mo Co-Doped SrTiO₃ as Novel Anode Material for Solid Oxide Fuel Cell Applications. In *Proceedings of the Advanced Functional Materials and Devices, Singapore, 2022*, 2022; 283-292, https://link.springer.com/chapter/10.1007/978-981-16-5971-3_31.
43. Cai, W.; Cao, D.; Zhou, M.; Yan, X.; Li, Y.; Wu, Z.; Lü, S.; Mao, C.; Xie, Y.; Zhao, C.; et al. Sulfur-tolerant Fe-doped La_{0.3}Sr_{0.7}TiO₃ perovskite as anode of direct carbon solid oxide fuel cells. *Energy* **2020**, *211*, 118958, <https://doi.org/10.1016/j.energy.2020.118958>.
44. Kosaka, F.; Nakamura, T.; Otomo, J. Electrochemical ammonia synthesis using mixed protonic-electronic conducting cathodes with exsolved Ru-nanoparticles in proton conducting electrolysis cells. *Journal of the Electrochemical Society* **2017**, *164*, F1323, <https://doi.org/10.1149/2.0401713jes>.

45. Sakai, T.; Matsushita, S.; Matsumoto, H.; Okada, S.; Hashimoto, S.; Ishihara, T. Intermediate temperature steam electrolysis using strontium zirconate-based protonic conductors. *International Journal of Hydrogen Energy* **2009**, *34*, 56-63, <https://doi.org/10.1016/j.ijhydene.2008.10.011>.
46. Ling, Y.; Yu, J.; Lin, B.; Zhang, X.; Zhao, L.; Liu, X. A cobalt-free $\text{Sm}_{0.5}\text{Sr}_{0.5}\text{Fe}_{0.8}\text{Cu}_{0.2}\text{O}_{3-\delta}$ - $\text{Ce}_{0.8}\text{Sm}_{0.2}\text{O}_{2-\delta}$ composite cathode for proton-conducting solid oxide fuel cells. *Journal of Power Sources* **2011**, *196*, 2631-2634, <https://doi.org/10.1016/j.jpowsour.2010.11.017>.
47. Orozco, C.; Melendez, A.; Manadhar, S.; Kongara, S.R.S.; Reddy, M.; Gandha, K.; Niebedim, I.C.; Ramana, C.V. Effect of Molybdenum Incorporation on the Structure and Magnetic Properties of Cobalt Ferrite. *The Journal of Physical Chemistry* **2017**, *121*, 25463-25471, <https://doi.org/10.1021/acs.jpcc.7b08162>.
48. Qiao, L.; Duan, G.; Zhang, S.; Ren, Y.; Sun, Y.; Tang, Y.; Wan, P.; Pang, R.; Chen, Y.; Russell, A.G.; et al. Electrochemical ammonia synthesis catalyzed with a CoFe layered double hydroxide – A new initiative in clean fuel synthesis. *Journal of Cleaner Production* **2020**, *250*, 119525, <https://doi.org/10.1016/j.jclepro.2019.119525>.
49. Da Silva, L.F.; Avansi, W.; Moreira, M.L.; Mesquita, A.; Maia, L.J.; Andrés, J.; Longo, E.; Mastelaro, V.R. Relationship between Crystal Shape, Photoluminescence, and Local Structure in SrTiO_3 Synthesized by Microwave-Assisted Hydrothermal Method. *Journal of Nanomaterials* **2012**, *2012*, <https://doi.org/10.1155/2012/890397>.
50. Nunocha, P.; Kaewpanha, M.; Bongkarn, T.; Phuruangrat, A.; Suriwong, T. A new route to synthesizing La-doped SrTiO_3 nanoparticles using the sol-gel auto combustion method and their characterization and photocatalytic application. *Materials Science in Semiconductor Processing* **2021**, *134*, 106001, <https://doi.org/10.1016/j.mssp.2021.106001>.
51. Lan, R.; Tao, S. Electrochemical synthesis of ammonia directly from air and water using a $\text{Li}^+/\text{H}^+/\text{NH}_4^+$ mixed conducting electrolyte. *RSC Advances* **2013**, *3*, 18016-18021, <https://doi.org/10.1039/C3RA43432J>.
52. Lan, R.; Alkhazmi, K.A.; Amar, I.A.; Tao, S. Synthesis of ammonia directly from wet air at intermediate temperature. *Applied Catalysis B: Environmental* **2014**, *152-153*, 212-217, <https://doi.org/10.1016/j.apcatb.2014.01.037>.
53. Amar, I.A.; Lan, R.; Humphreys, J.; Tao, S. Electrochemical synthesis of ammonia from wet nitrogen via a dual-chamber reactor using $\text{La}_{0.6}\text{Sr}_{0.4}\text{Co}_{0.2}\text{Fe}_{0.8}\text{O}_{3-\delta}$ - $\text{Ce}_{0.8}\text{Gd}_{0.18}\text{Ca}_{0.02}\text{O}_{2-\delta}$ composite cathode. *Catalysis Today* **2017**, *286*, 51-56, <https://doi.org/10.1016/j.cattod.2016.09.006>.
54. Kordali, V.; Kyriacou, G.; Lambrou, C. Electrochemical synthesis of ammonia at atmospheric pressure and low temperature in a solid polymer electrolyte cell. *Chemical Communications* **2000**, 1673-1674, <https://doi.org/10.1039/b004885m>.
55. Amar, I.A.; Lan, R.; Tao, S. Synthesis of ammonia directly from wet nitrogen using a redox stable $\text{La}_{0.75}\text{Sr}_{0.25}\text{Cr}_{0.5}\text{Fe}_{0.5}\text{O}_{3-\delta}$ - $\text{Ce}_{0.8}\text{Gd}_{0.18}\text{Ca}_{0.02}\text{O}_{2-\delta}$ composite cathode. *RSC Advances* **2015**, *5*, 38977-38983, <https://doi.org/10.1039/c5ra00600g>.
56. Zhang, S.; Duan, G.; Qiao, L.; Tang, Y.; Chen, Y.; Sun, Y.; Wan, P.; Zhang, S. Electrochemical Ammonia Synthesis from N_2 and H_2O Catalyzed by Doped LaFeO_3 Perovskite under Mild Conditions. *Industrial & Engineering Chemistry Research* **2019**, *58*, 8935-8939, <https://doi.org/10.1021/acs.iecr.9b00833>.